Research on the Development of Permanent Magnetic Gas Suspension Bearing in ORC Waste Heat Generator

Gang Zhang, Caiqin Xie, Kunpeng Yuan, Xuan Song, Jinman Xu, Dian Zhou

Research Institute of Mechanical Design and Bearing, School of Mechatronic Engineering and Automation, Shanghai University, Shanghai 200072, China, zg@shu.edu.cn

***Abstract*—High efficiency permanent magnet generator has been widely used in various applications due to its advantages of simple structure, high reliability, small size and high efficiency. However, under high speed condition, the energy loss of unit volume is increased by the mechanical friction generated for the traditional permanent magnet generator when using mechanical bearings. At the same time, oil and grease are not allowed to be used as lubricants in some ORC special occasions, so non-contact bearings are needed to replace mechanical bearings in high speed permanent magnet generators. The main objective of this paper is to develop a new type of permanent magnet gas suspension bearing and apply it to 200kW ORC waste heat permanent magnet generator. According to the specific condition of ORC waste heat permanent magnet generator to choose the appropriate structure of permanent magnetic bearing and gas bearing, and then considering the theory of porous hydrostatic gas bearing with generator and permanent magnet bearing (PMB) size to design the matching gas bearing. Meanwhile, in order to meet the requirement of strength and life, the 3D printing technology was applied to make the gas bearing liner with bearing which is a pioneer work. Then the whole structure design of the permanent magnet gas suspension bearing and the assemble of the bearing loading the ORC residual heat permanent magnet generator are done systematically. The simulation and experiment show that the development and design of ORC Waste Heat Generator supported by permanent magnet gas suspension bearing satisfy the design requirements.**

In recent years, along with the prices of international energy rising continuously, energy and environment problem in China is facing a growing challenge, at the same time in the face of increasing awareness of sustainable development and attaching importance to social benefits, power generation potential and economic prospect of low-temperature waste heat resources is gaining more and more attention, which has always been the most abundant resources and been not seen as the economical efficiency of power generation. Organic Rankine's Cycle (ORC) is a Organic Rankine's circulation with low boiling point organic matter as working medium, which mainly consist of the waste heat boiler (or heat exchanger), turbine, condenser, and working medium pump. Using working medium is the fundamental difference between ORC power generation system and traditional low-temperature waste heat generation system, and the pentapropane is used as working fluid in ORC working environment actually. The pentapropane is a colorless transparent easily flowing liquid, which is volatile. When it is above 58 C, it becomes a high pressure gas, which is insoluble with water and can be mixed with most organic solvents such as oil, hydrocarbon and so on. It will react with grease and lubricating oil, damaging bearing lubrication, so ORC waste heat generator rotors can't be supported by rolling bearings and sliding bearings lubricated with grease, or oil. In this paper, a permanent magnetic bearing with gas suspension bearing as auxiliary support or a new type of permanent magnet gas suspension bearing is developed as the supporting bearing of ORC waste heat generator. It can not only make full use of the existing pentapropane as gas source, but also overcome the disadvantage of short life of mechanical bearings in ORC condition of environment.

A. Parameters of Generator Rotation

In the vertical ORC waste heat permanent magnet generator system, the permanent magnetic bearing and the gas bearings are the key supporting parts. The generator is used for the power generation of industrial waste heat recycling. The working rotational speed is 18000rpm, the rated power is 200kW and the efficiency of generator is no less than 90%. The two ends of the generator are connected to the turbine impeller separately, and the bearing system is mainly subjected to the gravity of the rotor system in the non-working state, and the direction is downward along the axis. The high speed rotating turbine produces the aerodynamic force of 340kg in the working state. Because of the symmetrical connection of impellers in the two ends of the generator, the aerodynamic force cancels each other in ideal condition. At this time, the permanent magnetic bearing system mainly bears the gravity of the rotor. The fluctuating load of 10 ~ 20% aerodynamic force in axial can't be offset each other in the non-ideal working condition with unstable atmospheric pressure, and the axial load is 34~68kg (333.2~666.4N). The generator rotor adopts embedded permanent magnet structure, the material is rare earth NdFeb-38SH. The stator core is made of silicon steel sheet with 0.5mm thickness. Table I lists the parameters of each part of the rotor.

TABLE I. PARAMETERS OF ROTATION PART IN THE GENERATOR

Parameter / Model	Volume V/cm^3	Material	Mass m/kg
Central axis	1786.81	45	14.03
Rotor	2955.55	Silicon Steel Sheet	23.20
Permanent magnet	1502.68	NdFeB	11.80
Rotor sleeve	411.67	Carbon Fibre T600	0.73
Compounding			49.76

It can be seen that the weight of the rotating part of the generator is 49.76kg from Table I, while the actual rotating part also comprises two impellers, a flat key, a pin, and a shaft

sleeve moving magnetic ring seat, a thrust collar in the permanent magnet gas suspension bearing. Thus, the permanent magnet bearing should be suspended when bearing load is 60kg (588N) in the following design. The outer diameter of the permanent magnet gas suspension bearing is required to be smaller than the outer diameter of the generator stator, and the inner diameter of the permanent magnetic gas suspension bearing is greater than the outer diameter of the rotor shaft, so as to improve the critical speed of the rotor, and the height of the permanent magnet gas suspension bearing should be as small as possible.

B. Axial PMB Design

The structure of axial PMB is as shown in Fig.1.

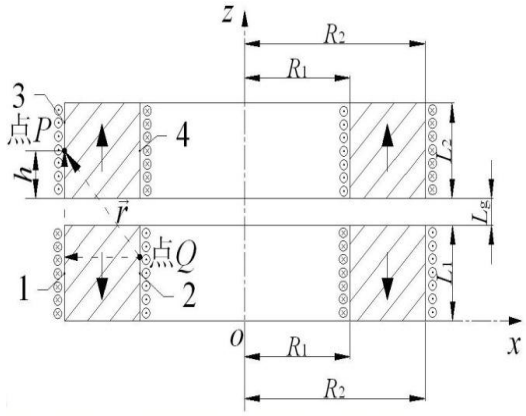

Figure 1. Structure of Axial PMB

PMB achieve a stable suspension by relying on magnetic force mainly between the magnetic rings, its bearing capacity is actually the magnetic force between the magnetic rings, so the calculation of the bearing capacity of the PMB ultimately comes down to the calculation of magnetic force between the magnetic rings. At present, there are three methods for magnetic force analysis: Equivalent Magnetic Charge Method (EMCM), Molecular Current Method (MCM), and Finite Element Method (FEM). The calculation results of MCM are closer to the experimental results than EMCM, and the results of FEM are the closest to the experimental results. Therefore, a preliminary calculation can be performed based on the formula developed by the (MCM) to determine the size of PMB. MCM solves formula as follows:

$$F_{13,z}=\frac{\mu_0 H_{c1}H_{c2}R_2^2}{4\pi}\cdot\int_0^{2\pi}\int_0^{2\pi}\int_0^{L_2}\int_{h+L_g}^{h+L_g+L_1}\frac{z\left(\sin\theta\sin\phi+\cos\theta\cos\phi\right)d\theta d\phi dzdh}{\left[\left(R_2\cos\phi-R_1\cos\theta\right)^2+\left(R_2\sin\phi-R_1\sin\theta\right)^2+z^2\right]^{3/2}} \tag{1}$$

$$F_{14,z}=-\frac{\mu_0 H_{c1}H_{c2}R_1R_2}{4\pi}\cdot\int_0^{2\pi}\int_0^{2\pi}\int_0^{L_2}\int_{h+L_g}^{h+L_g+L_1}\frac{z\left(\sin\theta\sin\phi+\cos\theta\cos\phi\right)d\theta d\phi dzdh}{\left[\left(R_2\cos\phi-R_1\cos\theta\right)^2+\left(R_2\sin\phi-R_1\sin\theta\right)^2+z^2\right]^{3/2}} \tag{2}$$

$$F_{23,z}=-\frac{\mu_0 H_{c1}H_{c2}R_1R_2}{4\pi}\cdot\int_0^{2\pi}\int_0^{2\pi}\int_0^{L_2}\int_{h+L_g}^{h+L_g+L_1}\frac{z\left(\sin\theta\sin\phi+\cos\theta\cos\phi\right)d\theta d\phi dzdh}{\left[\left(R_2\cos\phi-R_1\cos\theta\right)^2+\left(R_2\sin\phi-R_1\sin\theta\right)^2+z^2\right]^{3/2}} \tag{3}$$

$$F_{24,z}=\frac{\mu_0 H_{c1}H_{c2}R_1^2}{4\pi}\cdot\int_0^{2\pi}\int_0^{2\pi}\int_0^{L_2}\int_{h+L_g}^{h+L_g+L_1}\frac{z\left(\sin\theta\sin\phi+\cos\theta\cos\phi\right)d\theta d\phi dzdh}{\left[\left(R_2\cos\phi-R_1\cos\theta\right)^2+\left(R_2\sin\phi-R_1\sin\theta\right)^2+z^2\right]^{3/2}} \tag{4}$$

According to the principle of "same magnetic charges are repulsive and opposite magnetic charges are attractive", it can be seen that F_{13}'z and F_{24}'z take a negative value in the coordinate system of Fig.1, and F_{23}'z and F_{14}'z should take a positive value. Therefore, the sum of the axial magnetic forces for the lower magnetic ring to the upper magnetic ring is:

$$F_z=F_{23,z}+F_{14,z}-F_{13,z}-F_{24,z} \tag{5}$$

The symbol indicates the direction of the force, which positive means that the magnetic force is a repulsive force upward, and negative means that the magnetic force is downward suction. At the same time, axial stiffness can also be calculated:

$$K_z=\frac{dF_z}{dz} \tag{6}$$

It means the axial bearing capacity increases as the axial displacement increases when the axial stiffness is positive, so the magnetic force for axial freedom is stable conversely, the axial stiffness is negative and the magnetic force in axial is unstable.

In the above analysis, the requirements for capacity of PMB are given, and the basic structure of PMB is also determined. Therefore, we use the structure of a double magnetic rings, the size of the inner diameter R_1 is 37.5mm, outer diameter R_2 is 49.5mm, the thickness of the magnetic rings L_1, L_2 are all 12.0mm, the initial gap of the magnetic rings is 3mm. Fig.2 is the mechanical characteristic curve of the permanent magnet rings based on the formula calculated by MCM.

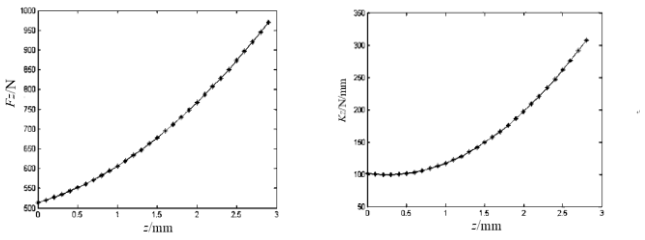

(a) (b)

Figure 2. Permanent magnetic ring axial mechanical characteristics curve

Fig.2(a) is a graph showing the load-bearing characteristics of permanent magnet rings, and Fig.2(b) is a graph of its stiffness characteristics. From the calculation results, it can be seen that the air gap gradually decreases from 3mm to 0.1mm (z = 0 ~ 2.9mm) in the process, the bearing capacity increased from 520N to 970N for the PMB of double magnetic rings, so in the air gap of about 2mm (z=1mm) to meet the bearing requirements of 588N. It indicates good axial stability while

the stiffness curve shows that the stiffness is getting larger, so the size of the magnetic ring basically meets the design requirements, the magnetic force calculated by MCM is consistent with the experimental value, but there is still a gap, so we need to use more exact FEM analyzes the specific working gap of the size magnetic ring after determining the size of the magnetic ring.

Analyzing the actual working gap of the magnetic ring by ANSYS software. Fig.3 shows the ANSYS analysis result of the magnetic force between two magnetic rings when the axial gap is 1.5mm, where fig.3(a) is the finite element model of the PMB, fig.3(b) is the magnetic force line vector figure, and fig.3(c) is a graph of the magnetic density of nodes. The repulsive force output by the magnetic ring at a clearance of 1.5mm is 590.10N seen from the result of ANSYS calculation on Fig.3(d), which is almost as same as the gravity of the actual rotating part. Therefore, the actual working gap of the magnetic ring is determined to be 1.5mm.

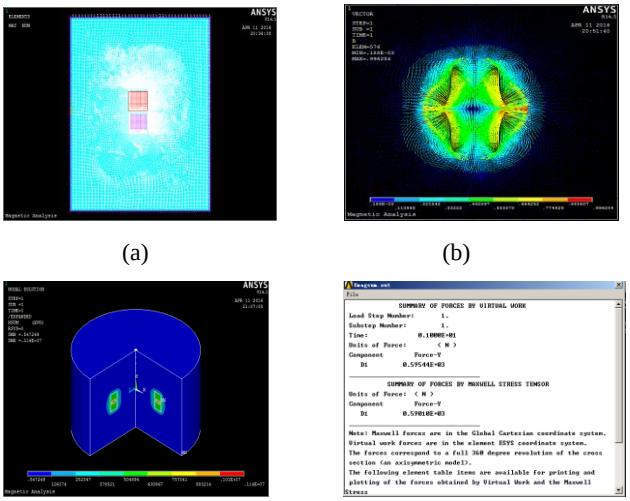

Figure 3. Finite element simulation analysis of two-ring PMB

PMB is a high-performance bearings that use a magnetic field force generated by a permanent magnet to suspend the rotor in the air without any mechanical contact between the rotor and the stator[1]. It has good load-bearing characteristics and stiffness characteristics in the main bearing direction, but it can't achieve permanent magnet suspension of all degree of freedom, so it is necessary to introduce auxiliary support in the design process of the PMB. Due to the ORC waste heat generator is used for industrial waste heat Recycling link with a stable supply of gas, its organic solvent pentafluoropropane and lubricating oils and greases will react chemically to destroy the lubrication of rolling bearings and oil-lubricated sliding bearings, so the auxiliary bearings should not be the rolling bearings and oil-lubricated sliding bearings. Gas suspension bearings are used as auxiliary supports eventually[2].

C. Design of Gas Suspension Bearing

As the porous material of porous gas suspension bearing, besides its anisotropy, the distortion of the pores of the material caused by manufacturing such as machining and heat treatment, local blockage, etc, add to the complexity of fluid flow. For this reasons, some necessary assumptions must be made to establish a physical model that can reflect actual working conditions and facilitate theoretical analysis[3]. A one-dimensional capillary model is used in this paper. With this model, that the porous layer is regarded as composition of numerous parallel capillary tubes arranged in the same direction in close proximity. The flow of gas between them can be viewed as one-dimensional flow along the capillary, flow direction and the surface of bearing is vertical. The quantity of flow is shown as below[4]:

$$q_m = -\frac{N_i \pi d_i^4 s}{128\mu}\frac{dp}{dz} \tag{7}$$

Air permeability coefficient is:

$$\phi = \frac{N_i \pi d_i^4}{128} \tag{8}$$

N_i is capillary number, d_i is capillary diameter in this formula.

To design a porous gas bearing, the materials and processing technology of porous materials should be selected. When the structure and size of the bearing are further determined, an "permeability parameter" Λ_ϕ that determines the basic parameters of the gas bearing is determined. The static, dynamic performances of porous hydrostatic gas bearing are determined mainly by the permeability parameter Λ_ϕ. However, to determine the compliance of bearing performance to Λ_ϕ, and seeking the optimization domain of Λ_ϕ for bearing performance, are the center task and the key of the porous bearings design[5].

The permeability parameters is defined as:

$$\Lambda_\phi = \frac{12 R_0^2 \phi}{H h_0^3} \tag{9}$$

The pressure function is obtained by differential calculation, and then the pressure function is integrated to obtain static characteristics such as dimensionless bearing capacity and stiffness as follows:

Bearing capacity:

$$\bar{W} = \frac{W}{\pi R_0^2 (p_s - p_a)} = \frac{2}{\bar{p}_s - 1}\int_0^1 (\bar{p} - 1)\bar{r}d\bar{r} \tag{10}$$

Stiffness:

$$\bar{K} = \frac{K\bar{k}h_0}{\pi R_0^2 (p_s - p_a)} = 3\Lambda_\phi \frac{d\bar{W}}{d\Lambda_\phi} \tag{11}$$

Fig.4 shows the change curves of dimensionless load $\bar{W}$ to permeability parameters Λ_ϕ.

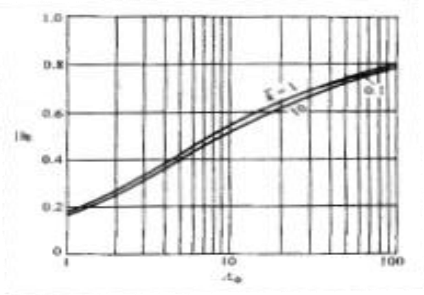

Figure 4. Affection curve of porous thrust bearing k on W- Λ_ϕ

According to the actual operating conditions, the one-dimensional capillary model is chosen. Because the radial perturbation force is symmetric and small, this paper focuses on the design of thrust bush in hydrostatic gas bearing.

Because the porosity of thrust bush is 20%, the inner diameter of the capillary d_i is 0.5mm. The number of pore on the thrust bush N_i is 14514, and the air permeability coefficient can be obtained from formula (8). Because the out radius of the thrust bush R_o is 51mm, inner radius R_i is 36.5mm, the thickness of the porous layer H is 4mm, and the nominal gap h_0 is 5×10^{-3}mm, gas supply pressure p_s-p_a is 0.5MP. Permeability parameters Λ_ϕ is 42.372 according to the definition of permeation parameters, the dimensionless load $\overline{W}$ can be obtained as 0.72 from the Fig.4, The capacity of thrust bearing is $W=\pi(R_0^2-R_i^2)\cdot(p_s-p_a)\overline{W}$=1435N (146Kgf) according to formula (10). It is much larger than the disturbance force generated by the aerodynamic force (666.4N) in the non-ideal working condition. Therefore, this thrust bush can produce a gas film under the ventilation state to provide a protection and avoid accidents. The bearing capacity of radial gas bearing W_r can be calculated as 2184N with the same method. For medium and large generator rotor, the dynamic balance precision grade should be G2.5, thus the eccentric distance of the rotor can be obtained, $e=\frac{G\cdot1000}{\omega}(\mu m)=\frac{G}{1000\omega}(m)$,eccentric force of the rotor is $F_c=Me\omega^2=M\frac{G}{1000\omega}\omega^2=\frac{MG\omega}{1000}=\frac{\pi nMG}{30000}=283N$ when the quality of the rotor is 60kg and it's rotate speed is 18000rad/min. The eccentric force (283N) is far less than the bearing capacity (2184N) of radial gas bearing. Therefore, the gas film produced by this bearing can play a radial locating and assistant control role under the ventilation condition when gas supply pressure (p_s-pa) is 0.5MP.

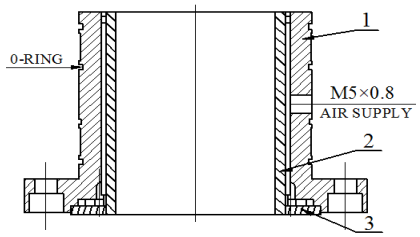

Figure 5. Diameter axial gas bearing

In the Fig.5 of radial axial gas bearings，1 is bearing back, 2 is lined bearing bush, and 3 is thrust bush. Auxiliary mechanical bearings in the PMB are equivalent to the mechanical control part of the active magnetic bearings. So PMB controlled by auxiliary mechanical bearings is chosen due to the cost of active magnetic bearings is too high. Considering comprehensively, we finally chose porous hydrostatic gas suspension bearings as auxiliary bearings. The main reason is though a ready-made high-pressure gas source can be used, but the gas source is not stable in the harsh environment. We have purchased imported South Korean air suspension bearings, it's lined bearing bush is made of carbon, but the strength cannot meet the actual working conditions. Therefore, the metal material is chosen and the 3D printing technology[6] is applied to make the lined bearing bush. At the same time, a small amount of special grease is applied in the lined bearing bush and on the thrust bush. There are Nano Ceramic Powders in the grease, which can form a 1~5μm thick wear-resistant ceramic film on the radial lined bush and the axial thrust bush. When the rotor rotates at high speed, the surfaces of the lined bearing bush and the thrust bush can withstand the impact and friction to improve the life of air-suspension bearings.

Porous gas suspension bearings have been using porous metal powders as the main raw material, and metal powder metallurgy processes have been used to make the lined bearing bush and thrust bush of porous gas suspension bearings. However, porous metal powder metallurgy must make mould for mass production, the cost of making test samples is too high, so metal 3D printing technology is applied to produce the porous lined bearing bush and thrust bush. Porous gas suspension bearings have not yet been widely used in the industrial field, and the adoption of metal 3D printing technology has made breakthroughs in the manufacture of gas bearings. 3D printing technology, with the feature of digitization, networking, personalization and customization, is rapidly changing traditional production methods and lifestyles, which is bound to promote the fourth industrial revolution. This is the first application of 3D printing technology in gas bearings, breaking the traditional simple printing rules. Fig.6 shows that the porous thrust bush and the lined bearing bush with a diameter of capillary tube d_i is 0.5mm, produced with 3D printing technology in the high-temperature blade center of the State Key Laboratory of Modern Metallurgy and Materials Preparation in Shanghai University.

(a) (b)

Figure 6. 3D printed thrust bush and lined bearing bush

D. Design and Application of Permanent Magnet Gas Suspension Bearing

The permanent magnet gas suspension bearing is composed of permanent magnet bearing and porous gas suspension bearing. The permanent magnet bearing utilizes magnetic force

between the magnetic rings to achieve stale suspension, and its bearing capacity is used to support the weight of rotating parts of the generator rotor and the rotating shaft. The porous gas suspension bearing utilizes on-site gas supply to form a gas film to achieve radial positioning assisting control and axial limit protection. Therefore, the specific structure of the permanent magnet gas suspension bearing designed for ORC waste heat generator is shown in Fig.7.

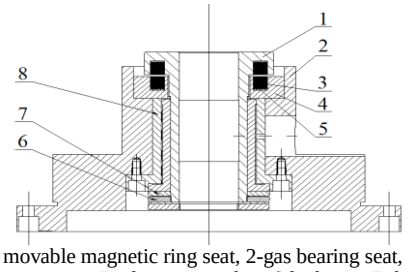

1- bushing movable magnetic ring seat, 2-gas bearing seat, 3-magnetic ring, 4-fixing magnet ring seat, 5-adjustting gasket, 6-lock nut, 7-thrust bush, 8-gas bearing

Figure 7. Specific structure of the permanent magnet gas suspension bearing

The virtual assembly of the permanent magnet gas suspension bearing is shown in Fig.8(a). and the actual assembled drawing is shown in Fig.8(b). The gas bearing and the movable magnetic ring seat adopt clearance fit. Fig.8(c) is a actual object of the upper gas suspension bearing, which is composed of a gas bearing, an upper gas bearing seat and an upper bearing sleeve. Fig.8(d) is an assembly drawing of a rotor shaft mounted on a permanent magnet gas suspension bearing. Fig.8(e) is an assembly drawing of a permanent magnet air suspension bearing applied in an ORC waste heat generator. Fig.8(f) is an external view of an ORC waste heat generator supported by a permanent magnet gas suspension bearing.

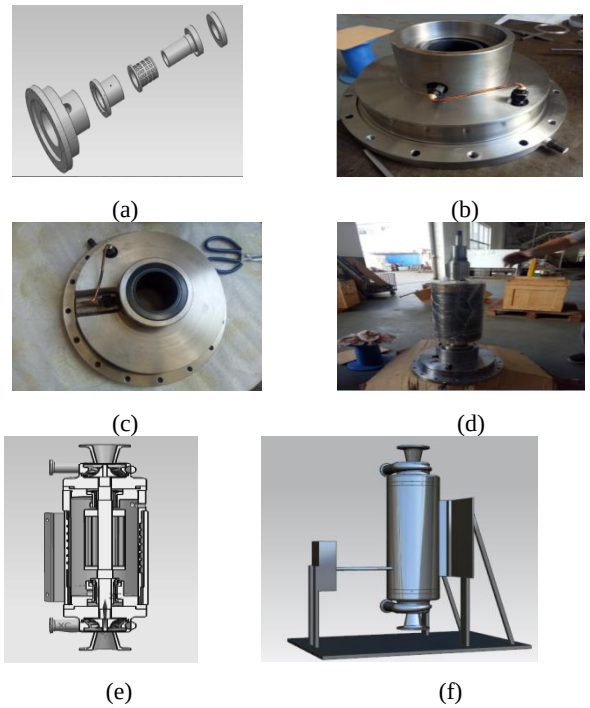

(a) (b) (c) (d) (e) (f)

Figure 8. Virtual assembly of permanent magnet gas suspension bearing and generator

E. *Dynamic Analysis of ORC Waste Heat Generator*

The stiffness K_r of the porous hydrostatic gas radial bearing is 109200 N/mm. PMB have an axial stiffness K_{a1} is 150 N/mm, and the stiffness K_{a2} of the axial-gas-suspension thrust-bush is 13605 N/mm, so the axial stiffness K_a is 13755 N/mm which is the sum of the PMB stiffness and the axial gas suspension thrust bush stiffness. The modal analysis modules of ANSYS-Workbench is shown in Fig.9(a). Then inputting of related parameters is shown in Fig.9(b) and designing of the boundary conditions is shown in Fig.9(c).

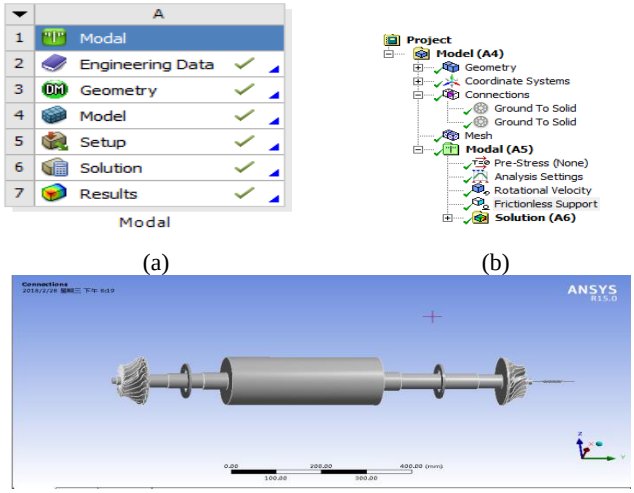

(a) (b)

(c)

Figure 9. Workbench pre-processing diagram

The first eight vibration modes are extracted to analyze. The vibration modes of rotor system are shown in Fig.10.

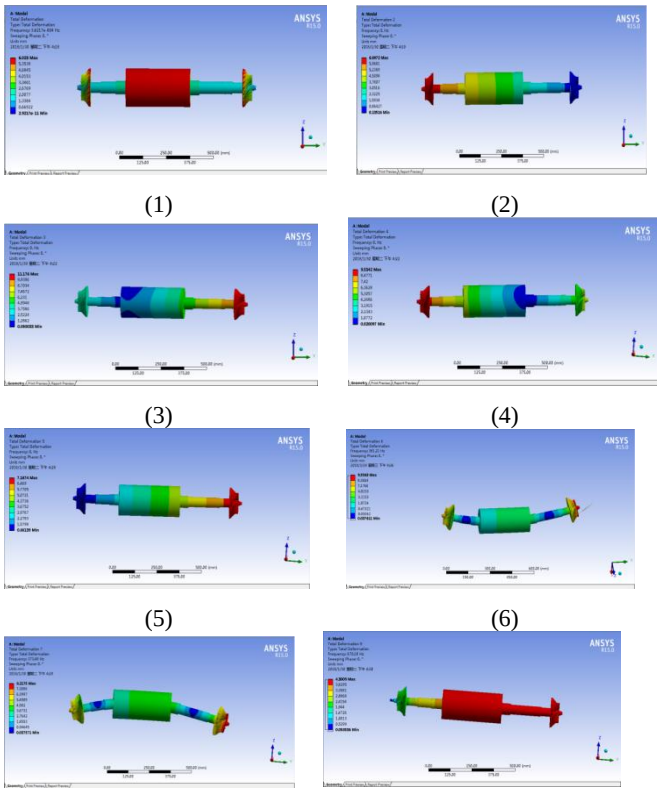

(1) (2) (3) (4) (5) (6) (7) (8)

Figure 10. The f irst 8 order critical speed vibration modes

After running and calculation, the natural frequency of the first 10 orders is shown in Table II.

TABLE II. THE NATURAL FREQUENCY OF ROTOR SYSTEM

Mode	Frequency [Hz]	Rotate Speed[r/min]
1.	3.6217e-004	0
2.	0.	0
3.	0.	0
4.	0.	0
5.	0.	0
6.	381.21	22872.6
7.	382.21	22932.6
8.	674.63	40477.8
9.	826.36	49581.6
10.	828.34	49700.4

Table II shows the natural frequency results of the first 10 orders of the bearing rotor system. It can be seen that the modal frequencies of the 1st to 5th order are 0 Hz, and it is corresponding to the rigid body motion of 4 degrees of freedom in the radial direction and 1 degree of freedom in the axial direction for the first five vibration modes of rotor system in Fig.10. The 6th and 7th modal frequencies are similar to 381.21Hz and 382.21Hz, respectively representing the vibration mode frequencies in two orthogonal radial directions. The eighth mode frequency is 674.63Hz corresponding to the vibration mode frequency of axial direction. The 9th and 10th modal frequencies are similar to 826.36 Hz and 828.34 Hz, representing the vibration mode frequencies of two orthogonal radial directions respectively[7].

Turn on the gyro effect and set the rotate speed value in Fig.11.

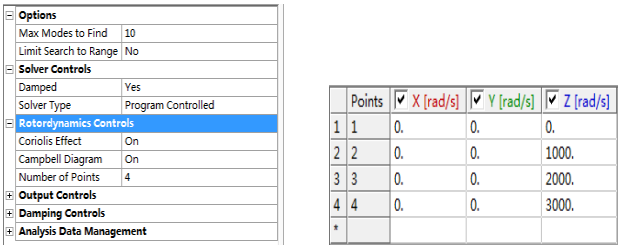

Figure 11. Turn on the gyro effect and set the rotate speed value

The Campbell curve[8] is drawn finally in Fig.12 as shown below:

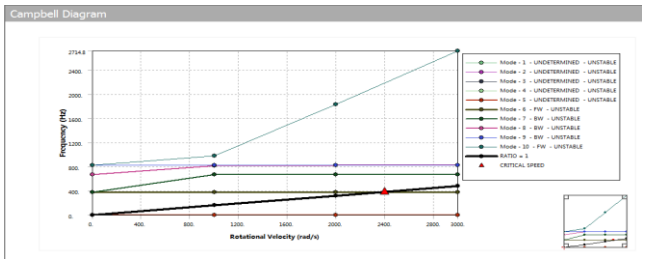

Figure 12. The Campbell curve

The rotor critical speed can be read as 2397.3 rad/s from the report preview as shown in fig.13. That is 22892.53 rpm.

Model (A4) > Modal (A5) > Solution (A6) > Campbell Diagram

Mode	Whirl Direction	Mode Stability	Critical Speed	0. rad/s	1000. rad/s	2000. rad/s	3000. rad/s
1.	UNDETERMINED	UNSTABLE	NONE	0. Hz	0. Hz	0. Hz	0. Hz
2.	UNDETERMINED	UNSTABLE	NONE	0. Hz	0. Hz	0. Hz	0. Hz
3.	UNDETERMINED	UNSTABLE	NONE	0. Hz	0. Hz	0. Hz	0. Hz
4.	UNDETERMINED	UNSTABLE	NONE	0. Hz	0. Hz	0. Hz	0. Hz
5.	UNDETERMINED	UNSTABLE	NONE	0. Hz	0. Hz	0. Hz	0. Hz
6.	FW	UNSTABLE	2397.3 rad/s	381.21 Hz	381.54 Hz	381.54 Hz	381.54 Hz
7.	BW	UNSTABLE	NONE	382.21 Hz	674.63 Hz	674.62 Hz	674.62 Hz
8.	BW	UNSTABLE	NONE	674.63 Hz	815.54 Hz	822.45 Hz	822.94 Hz
9.	BW	UNSTABLE	NONE	826.36 Hz	827.03 Hz	827.15 Hz	827.17 Hz
10.	FW	UNSTABLE	NONE	828.34 Hz	983.69 Hz	1833.5 Hz	2714.8 Hz

Figure 13. Report preview

The first-order bending critical vibration frequency of the rotor system is 381.21 Hz, so its first-order bending critical rotation speed is 22892.53 rpm. It can be seen that the rotor will resonate at the first-order bending critical rotational speed 22892.53 rpm from Fig.10(6). The generator rotor radial maximum displacement is 3.6mm, less than 5mm gap between the motor rotor and the stator. Because the system's normal operating rotation speed is 18000rpm less than 0.8 times of the first-order bending critical speed, the rotor system is rigid axis and does not resonate. Thus it is safe at work.

F. Construction of Experimental Platform and Result of Test

A prototype of a vertical ORC waste heat generator supported by permanent magnetic gas suspension bearing with a rated power of 200kW and a rated rotational speed of 18000rpm is developed as shown in Fig.14(a). Fig.14(b) is the experimental schematic diagram, and Fig.14(c) is the experimental platform.

(a)

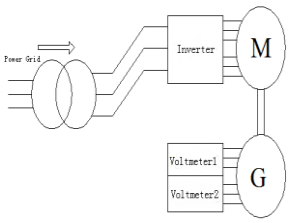

(b)

(c)

Figure 14. Vertical ORC waste heat generator supported by permanent magnetic gas suspension bearing

It is the experimental principle shown in Fig.14(b), the experimental platform is mainly composed of a three-phase asynchronous motor and a vertical ORC waste heat generator supported by the permanent magnetic gas suspension bearing developed in this paper shown in Fig.14(c). Three phase asynchronous motor is driven by frequency converter to simulate the power source of organic medium. The motor

transfers power to the ORC residual heat generator through the belt pulley. During the experiment, the generator is always in no load condition. The two voltmeters are connected at the outlet of the generator to measure the output voltage and compare the balance of the three phases.

The data obtained in preliminary operation of the experimental platform are shown in Table III.

TABLE III. ROTATIONAL SPEED AND VOLTMETER OF ORC WASTE HEAT GENERATOR

Input frequency (Hz)	Generator speed (rpm)	Output voltage 1 (V)	Output voltage 2 (V)	Average output voltage (V)
20	1503	30	32	3120
30	2256	47	48	47.5
40	3008	62.5	63	62.75
50	3765	79	79	79
60	4516	94.5	95	94.75
70	5260	110	109.5	109.75
75	5627	118	117.5	117.75
80	6004	126	126	126
85	6366	134	134	134
90	6738	142	143	142.5
95	7119	150	150	150
100	7479	158	158	158
105	7840	164	164	164
115	8564	180	179	179.5

According to the relation between the rotational speed of generator and the average output voltage in Table III, the relationship between them is fitted by software and the output voltage of 18000rpm and 20000rpm is calculated. The speed and voltage characteristic curve obtained after fitting is shown in Fig.15.

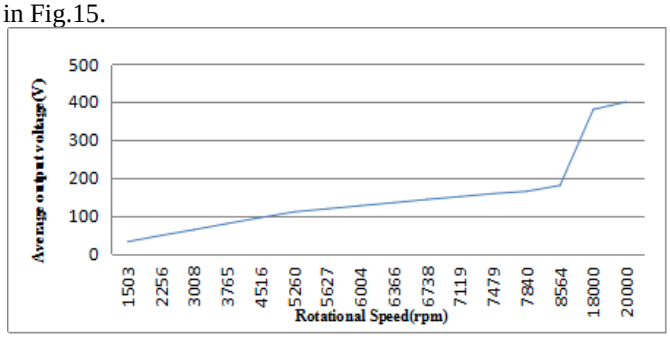

Figure 15. Diagram of relation between rotational speed and average output voltage

It can be concluded that there is a good linear relationship between the output voltage and the rotational speed of the ORC waste heat generator, and the 380V voltage can be output under the rated working speed of 18000rpm. The output voltage 1 and voltage 2 can be seen that the three-phase voltage of the generator is balanced, which meets the design requirements. Fig.16 is a practical application of ORC waste heat generator supported by permanent magnetic gas suspension bearing.

Figure 16. Application of ORC waste heat generator supported by permanent magnetic gas suspension bearing

G. Conclusion

In this paper, a vertical ORC waste heat generator is used as the research platform. The axial permanent magnetic gas suspension bearing is the research object. The application of the axial permanent magnetic gas suspension bearing in the vertical ORC waste heat generator is studied. The developed permanent magnetic gas suspension bearing is also used for the first time in the ORC waste heat generator. At present, there are no reports about the research results of permanent magnetic gas suspension bearing. Before studying the permanent magnetic gas suspension bearing, we used a rolling bearing as an auxiliary support[1], but the final failure is due to the bad ORC high temperature corrosion environment. Under the action of pentapropane gas, the grease would react with the working substance to produce residue, which destroys the lubrication of auxiliary support bearing, and the use of lubricating oil will be the same bad. It will not only consume a lot of lubricating oil in a short time, but also reduce the efficiency of the vaporization and expansion of the working material. From the cost point of view, neither grease nor oil can be used as lubricant for rotor supporting bearing of ORC waste heat generator. Therefore, we pioneered the development of the combination of gas bearing and permanent magnetic bearing as the bearing of the ORC waste heat generator. It can not only make full use of the industrial waste heat source, but also overcome the shortcomings of the short life of the rolling bearing in bad working conditions. By analyzing the critical speed and vibration mode of the rotor system and the Campbell curve, it is known that the 1st critical bending speed of the rotor is 22892.53r/min. The rotor's normal working speed is 18000rpm, less than 0.8 times of the 1st critical bending speed, so the system is safe under the running condition. Finally, a simple experimental platform is built. The experimental results show that ORC waste heat generator supported by permanent magnetic gas suspension bearing meets the design requirements and can be applied in practice.

H. Acknowledgement

The authors are very grateful for the support by the Project of Natural Science Foundation of China (51075251, 51175052).

REFERENCES

[1] Kuangyi Pei, "Research on the development of permanent magnetic bearing in ORC waste heat generator," *Academic Dissertation of Shanghai University*, pp. 69-70, 2016.

[2] Dian Zhou, “Research on the development of permanent magnetic air suspension bearing in ORC waste heat generator,” *Academic Dissertation of Shanghai University*, pp. 68-69, 2018.
[3] Yunfei Wang, “Research on static performance of porous hydrostatic bearings” *Machinery of Luoyang Bearing Research Institute* , 1982.
[4] Jinming Du, Zesheng Lu anJinming Du, Zesheng Lu and Yazhou Sun, “Comparison of micropore throttle and porous throttle” *Journal of Lubrication and Sealing*, vol. 10, no. 4, pp. 2–5, 2002.
[5] Shaojie Hua,Shaoming Fu and Hong Guo, “Finite element-optimized comprehensive analysis of dynamic and static sliding bearings with built-in capillary throttling” *Journal of Zhengzhou University of Technology*, vol. 17, no. 4, pp. 3–8, 1996.
[6] Hong Jiang, Xueping Kang,“Development of 3D printing technology” *Journal of New material industry*, vol. 10, no. 2, pp. 30–35, 2013.
[7] Xinrong He, Xingjun Fu, “Research on dynamic characteristics of bearing-rotor system based on ANSYS” *Journal of Mechanical research and application*, vol. 9, no. 6, pp. 39–41, 2012.
[8] Songsheng Li, Gang Zhang and Xiaoyang Chen, “Analysis of dynamic performance of high speed motorized spindle bearings-rotor system” *Journal of Mechanical Science and Technology*, vol. 25, no. 12, pp. 1447–1450, 2007.